^{99m}Tc- and ^{111}In-Labeled α-Melanocyte-Stimulating Hormone Peptides as Imaging Probes for Primary and Pulmonary Metastatic Melanoma Detection

Yubin Miao[1], Katherine Benwell[2], and Thomas P. Quinn[2–4]

[1]College of Pharmacy, University of New Mexico, Albuquerque, New Mexico; [2]Department of Biochemistry, University of Missouri-Columbia, Columbia, Missouri; [3]Department of Radiology, University of Missouri-Columbia, Columbia, Missouri; and [4]Harry S. Truman Memorial Veterans Hospital, Columbia, Missouri

It is highly desired to develop new imaging probes for early detection of melanoma as early diagnosis and prompt surgical removal are a patient's best hope for a cure. The purpose of this study was to determine whether ^{99m}Tc- and ^{111}In-labeled α-melanocyte-stimulating hormone (α-MSH) peptides could be used as imaging probes for primary and metastatic melanoma using dual-modality micro-SPECT/CT detection. **Methods:** [Cys^{3,4,10},D-Phe^7,Arg^{11}]α-MSH$_{3–13}$ [(Arg^{11})CCMSH] and [1,4,7,10-tetraazacyclododecane-1,4,7,10-tetraacetic acid]Re(Arg^{11})-CCMSH [DOTA-Re(Arg^{11})CCMSH] were labeled with ^{99m}Tc and ^{111}In. The pharmacokinetics of ^{99m}Tc-(Arg^{11})CCMSH were examined in B16/F1 flank and B16/F10 pulmonary metastatic murine melanoma-bearing C57 mice. The biodistribution of ^{111}In-DOTA-Re(Arg^{11})CCMSH was performed in B16/F10 pulmonary metastatic murine melanoma-bearing C57 mice. SPECT/CT of ^{99m}Tc-(Arg^{11})CCMSH and ^{111}In-DOTA-Re(Arg^{11})-CCMSH was determined in B16/F1 flank and B16/F10 pulmonary metastatic murine melanoma-bearing C57 mice. **Results:** ^{99m}Tc-(Arg^{11})CCMSH and ^{111}In-DOTA-Re(Arg^{11})CCMSH exhibited high tumor uptakes (14.03 ± 2.58 percentage injected dose/gram [%ID/g] at 1 h after injection and 17.29 ± 2.49 %ID/g at 2 h after injection) in B16/F1 melanoma-bearing mice, and the flank melanoma tumors were clearly imaged by micro-SPECT/CT. Nontarget organ uptakes were considerably lower except for the kidneys. B16/F10 pulmonary melanoma metastases were also clearly visualized by micro-SPECT/CT using ^{99m}Tc-(Arg^{11})CCMSH or ^{111}In-DOTA-Re(Arg^{11})CCMSH as the imaging probe. ^{99m}Tc-(Arg^{11})CCMSH exhibited images with greater resolution of metastatic melanoma lesions compared with ^{111}In-DOTA-Re(Arg^{11})CCMSH. **Conclusion:** The favorable tumor imaging properties of ^{99m}Tc-(Arg^{11})CCMSH and ^{111}In-DOTA-Re(Arg^{11})CCMSH highlighted their potential as novel probes for primary and metastatic melanoma detection.

Key Words: α-melanocyte-stimulating hormone; ^{99m}Tc- and ^{111}In-labeled peptides; primary and metastatic melanoma detection

J Nucl Med 2007; 48:73–80

Malignant melanoma is the sixth most commonly diagnosed cancer in the United States, with 62,190 new cases and 7,910 fatalities projected for the year 2006 (*1*). Currently, there is no cure for metastatic melanoma, as metastatic melanoma is resistant to current chemotherapy and immunotherapy regimens. The survival times for patients with disseminated metastatic melanoma average 3–15 mo (*2*). Early melanoma tumor diagnosis and prompt surgical removal are a patient's best hope for a cure. The basis for current clinical diagnosis of melanoma is built on the morphologies of melanoma, which includes asymmetry, border irregularity, color variegation, and diameter bigger than 6 mm. However, the diagnostic accuracy of melanoma is about 65% (*3*). Therefore, it is highly desired to develop new imaging probes for early detection of melanoma. At present, ^{18}F-FDG is the most commonly used in PET diagnosis and staging of cancer, including melanoma (*4*). Generally, ^{18}F-FDG exhibited increased accumulation in cancer cells because cancer cells have a higher metabolic rate than normal cells (*5*). However, ^{18}F-FDG is not melanoma-specific and it has been reported that some melanoma cells were undetectable by ^{18}F-FDG as they used substrates other than glucose as energy sources (*6*). Alternatively, radiolabeled α-melanocyte-stimulating hormone (α-MSH) peptide analogs are very promising imaging probes for melanoma detection. Radiolabeled α-MSH peptide analogs specifically bind to melanocortin-1 (MC1) receptors that are overexpressed on human and mouse melanoma cells (*7–12*), making radiolabeled α-MSH peptide analogs attractive targets in the diagnosis of melanoma.

Over the past several years, our laboratory has focused on developing radiolabeled α-MSH peptide analogs for melanoma detection and targeted radionuclide therapy (*9–13*). A novel class of metal cyclized α-MSH peptide analogs derived from the native α-MSH has been designed for melanoma targeting. Metal cyclization made the peptide analogs resistant to chemical and proteolytic degradation in vivo. The efforts focused on optimizing the pharmacokinetics

of the peptides yielded 2 novel peptide analogs with nanomolar binding affinities to MC1 receptors—namely, [Cys[3,4,10],D-Phe[7],Arg[11]]α-MSH[3–13] [(Arg[11])CCMSH] (11,12) and [1,4,7,10-tetraazacyclododecane-1,4,7,10-tetraacetic acid]Re(Arg[11])CCMSH [DOTA-Re(Arg[11])CCMSH] (14). The peptides were labeled with therapeutic radionuclides such as [188]Re and [212]Pb to examine their tumor-targeting properties and therapeutic efficacies in mouse melanoma models (15,16). Both [188]Re-(Arg[11])CCMSH and [212]Pb-DOTA-Re(Arg[11])CCMSH exhibited high receptor-mediated tumor uptakes and therapeutic efficacies in B16/F1 murine melanoma-bearing C57 mice. The tumor-targeting properties of the [188]Re-labeled (Arg[11])CCMSH and [212]Pb-labeled DOTA-Re(Arg[11])CCMSH peptides suggested that [99m]Tc-(Arg[11])CCMSH and ^{111}In-DOTA-Re(Arg[11])CCMSH would be strong candidates for melanoma imaging agents.

The development of high-resolution SPECT has enabled imaging of biochemical processes in small-animal models of disease noninvasively. The imaging quality of SPECT can be improved significantly by replacing the standard collimator with the pinhole collimator due to its magnification effect (17–22). Dual-modality imaging enables the simultaneous acquisition of both SPECT and CT images in the same spatial alignment. CT images can provide high-resolution anatomic information that makes the localization of radioactivity uptake regions more accurate (23). The benefits of combined functional and structural imaging are very attractive for melanoma detection. [99m]Tc and ^{111}In are widely used in most nuclear medicine facilities for diagnostic applications. [99m]Tc is an ideal isotope for SPECT because of its 140-keV γ-photon emission and 6-h decay half-life. [99m]Tc is very cost-effective and can be easily obtained from a [99]Mo-^{99m}Tc generator, facilitating its use for routine clinical imaging. [111]In is another attractive isotope for SPECT because of its 171- and 245-keV γ-photon emission. [111]In has a half-life of 2.8 d and is commercially available.

In this article, we describe the biodistribution studies and SPECT/CT of [99m]Tc-(Arg[11])CCMSH and ^{111}In-DOTA-Re(Arg[11])CCMSH in primary and pulmonary metastatic melanoma models to examine whether they are effective agents for both primary and metastatic melanoma detection by SPECT. Favorable pharmacokinetics and tumor-targeting properties highlighted the potential of [99m]Tc-(Arg[11])-CCMSH and ^{111}In-DOTA-Re(Arg[11])CCMSH as novel imaging probes for melanoma detection.

MATERIALS AND METHODS

Chemicals and Reagents

Amino acids and amide resin were purchased from Advanced ChemTech Inc. DOTA-tri-t-butyl ester was purchased from Macrocyclics Inc. [99m]Tc was obtained by eluting a [99]Mo-^{99m}Tc generator (Mallinckrodt, Inc.). [111]InCl$_3$ was purchased from Mallinckrodt, Inc. All other chemicals used in this study were purchased from Fischer Scientific and used without further purification.

B16/F1 Flank and B16/F10 Pulmonary Metastatic Melanoma Models

B16/F1 and B16/F10 murine melanoma cells (American Type Culture Collection) were cultured in RPMI 1640 medium (Invitrogen Corp.) containing NaHCO$_3$ (2 g/L), which was supplemented with 10% heat-inactivated fetal calf serum, 2 mmol/L L-glutamine, and 48 mg of gentamicin. B16/F1 flank melanoma tumors were generated by subcutaneously inoculating 1×10^6 B16/F1 cells in the right flank of C57 mice. The tumors reached approximately 0.2 g 10–12 d after cell implantation. Pulmonary metastatic melanoma tumors were generated by injecting 2×10^5 B16/F10 cells into C57 mice through the tail vein. The metastatic melanoma-bearing mice were used for biodistribution studies 16 d after cell injection.

Peptide Radiolabeling

The peptides (Arg[11])CCMSH and DOTA-Re(Arg[11])CCMSH were synthesized as described in the literature (10,13). ^{99m}Tc-labeled (Arg[11])CCMSH was prepared via a glucoheptonate transchelation reaction as described by Chen et al. (10). The radiolabeled peptide was purified by reverse-phase high-performance liquid chromatography (RP-HPLC) (Waters) on a C-18 reverse-phase analytic column (Vydac). A 20-min gradient of 18%–28% acetonitrile in H$_2$O/20 mmol/L HCl at a flow rate of 1 mL/min was used for radiolabeled peptide purification. ^{111}In-DOTA-Re(Arg[11])CCMSH was prepared according to the radiolabeling procedure described by Chen et al. (13). The radiolabeled complex was purified to a single species by RP-HPLC on a C-18 reverse-phase analytic column using a 20-min gradient of 16%–26% acetonitrile in 20 mmol/L HCl aqueous solution at a flow rate of 1 mL/min. The separation of excess nonradiolabeled peptides from radiolabeled peptides was monitored with an ultraviolet flow detector at a wavelength of 280 nm.

The purified peptide samples were purged with N$_2$ gas for 20 min to remove the acetonitrile. The pH of the final solution was adjusted to 5 with 0.1N NaOH and diluted with normal saline for animal studies. For imaging studies, the HPLC-purified radiolabeled (Arg[11])CCMSH peptide solution was concentrated through a Sep-Pak C18 column (3M Bioanalytical Technologies) and reconstituted with saline.

Biodistribution Studies

All the animal studies were conducted in compliance with Institutional Animal Care and Use Committee approval. The pharmacokinetics of [99m]Tc-(Arg[11])CCMSH was performed in B16/F1 murine melanoma-bearing C57 female mice (Harlan). Approximately 0.037 MBq of ^{99m}Tc-labeled peptide were injected into each mouse through the tail vein for biodistribution studies. Groups of 4 mice per each time point were used for the biodistribution studies. The mice were sacrificed at 1, 4, and 24 h after injection, and tumors and organs of interest were harvested, weighed, and counted. Blood values were taken as 6.5% of the whole-body weight. The results are expressed as percentage injected dose/gram (%ID/g) and as percentage injected dose (%ID). The tumor uptake specificities of [99m]Tc-(Arg[11])CCMSH were determined by blocking tumor uptake with the coinjection of 10 μg of unlabeled [Nle[4],D-Phe[7]]α-MSH (NDP), a linear α-MSH peptide analog with picomolar affinity for the MC1 receptor present on murine melanoma cells. The biodistribution of [99m]Tc-(Arg[11])CCMSH and ^{111}In-DOTA-Re(Arg[11])CCMSH at 2 and 4 h after injection was performed in B16/F10 pulmonary metastatic

murine melanoma-bearing and normal C57 female mice as described. Statistical analysis was performed using the Student t test for unpaired data. A 95% confidence level was chosen to determine the significance between compounds, with $P < 0.05$ being significantly different.

Primary and Metastatic Melanoma Imaging with ^{99m}Tc-(Arg^{11})CCMSH and ^{111}In-DOTA-Re(Arg^{11})CCMSH

B16/F1 melanoma-bearing C57 mice were injected separately with 27.75 MBq of ^{99m}Tc-(Arg^{11})CCMSH and 20.35 MBq of ^{111}In-DOTA-Re(Arg^{11})CCMSH via the tail vein 13 d after cell implantation. The mice were euthanized for micro-SPECT/CT at 2 h after injection. The SPECT data were collected immediately after CT data collection. Approximately 3.92 MBq of ^{99m}Tc-(Arg^{11})CCMSH and 2.22 MBq of ^{111}In-DOTA-Re(Arg^{11})CCMSH of radioactivity were present in the mice at the moment of acquisition, respectively. Micro-SPECT scans of 60 frames for each animal were acquired for total count acquisitions of 4 million counts for ^{99m}Tc-(Arg^{11})CCMSH and 5 million counts for ^{111}In-DOTA-Re(Arg^{11})CCMSH. B16/F10 pulmonary melanoma-bearing C57 mice were injected with 18.50 MBq of ^{99m}Tc-(Arg^{11})CCMSH and 37.00 MBq of ^{111}In-DOTA-Re(Arg^{11})CCMSH via the tail vein 24 d after cell injection. The mice were euthanized for micro-SPECT/CT at 2 h after injection. Approximately 2.89 MBq of ^{99m}Tc-(Arg^{11})CCMSH and 2.52 MBq of ^{111}In-DOTA-Re(Arg^{11})-CCMSH of radioactivity remained in the mice at the moment of acquisition, respectively. Micro-SPECT scans of 60 frames for each animal were acquired for total count acquisitions of 2 million counts for ^{99m}Tc-(Arg^{11})CCMSH and 5 million counts for ^{111}In-DOTA-Re(Arg^{11})CCMSH. The micro-SPECT images were obtained using the micro-CAT II SPECT/CT (Siemens Medical Solutions) unit equipped with high-resolution 2-mm pinhole collimators. The SPECT component of this preclinical imaging system was equipped with dual pixellated sodium iodide detectors. Each detector head was comprised of 10,000 NaI crystals ($1.25 \times 1.25 \times 5$ mm) arranged in a 100×100 crystal array coupled to 9 Hamamatsu position-sensitive photomultiplier tubes. The SPECT volumetric isotropic voxel data ($78 \times 78 \times 102$ matrix) was reconstructed using a 3-dimensional ordered-subset expectation maximization algorithm with geometric misalignment corrections. The CT component of this instrument was equipped with an 80-kVp x-ray source and appropriate software allowing 360° data acquisition. A cone beam (Feldkamp) filtered backprojection algorithm was used for reconstructing the CT raw projection data into a $512 \times 512 \times 960$ isotropic voxel image matrix. Reconstructed data from SPECT and CT were visualized and coregistered using Amira 3.1 (Ascent Media Systems & Technology Service).

RESULTS

The (Arg^{11})CCMSH and DOTA-Re(Arg^{11})CCMSH peptides were synthesized and purified by RP-HPLC, and the identities of the peptides were confirmed by electrospray ionization mass spectrometry. (Arg^{11})CCMSH and DOTA-Re(Arg^{11})CCMSH were radiolabeled with ^{99m}Tc and ^{111}In, respectively. ^{99m}Tc-(Arg^{11})CCMSH and ^{111}In-DOTA-Re(Arg^{11})CCMSH were completely separated from their nonradiolabeled excess peptides by RP-HPLC. The retention times of ^{99m}Tc-(Arg^{11})CCMSH and ^{111}In-DOTA-Re(Arg^{11})CCMSH were 17.1 and 15.2 min, respectively. The specific activities of ^{99m}Tc-(Arg^{11})CCMSH and ^{111}In-DOTA-Re(Arg^{11})CCMSH were 1.2135×10^{10} MBq/g and 8.1164×10^8 MBq/g, respectively. Illustrations of ^{99m}Tc-(Arg^{11})CCMSH and ^{111}In-DOTA-Re(Arg^{11})CCMSH structures are shown in Figure 1.

The pharmacokinetics and tumor targeting properties of ^{99m}Tc-(Arg^{11})CCMSH were determined in B16/F1 murine melanoma-bearing C57 mice. The biodistribution of ^{99m}Tc-(Arg^{11})CCMSH is shown in Table 1. The biodistribution of ^{111}In-DOTA-Re(Arg^{11})CCMSH in B16/F1 melanoma-bearing C57 mice was cited from Cheng et al. (*14*) and is included in Table 1 for comparison. Statistical analysis of ^{99m}Tc-(Arg^{11})CCMSH and ^{111}In-DOTA-Re(Arg^{11})CCMSH was performed with the Student t test for unpaired data. ^{99m}Tc-(Arg^{11})CCMSH exhibited high tumor uptake and extended retention. At 1 h after injection, 14.03 ± 2.58 %ID/g of activity accumulated in the tumors. Approximately 11.16 ± 1.77 %ID/g of activity remained in the tumors at 4 h after injection. The tumor uptake of ^{99m}Tc-(Arg^{11})CCMSH gradually decreased to 3.33 ± 0.50 %ID/g at 24 h after injection. Tumor uptake of ^{99m}Tc-(Arg^{11})CCMSH with coinjection of 10 μg of NDP was only 10% of the tumor uptake without NDP coinjection at 1 h after dose administration ($P < 0.05$), demonstrating that the uptake of radioactivity was receptor mediated. ^{99m}Tc-(Arg^{11})CCMSH and ^{111}In-DOTA-Re(Arg^{11})CCMSH displayed statistically similar tumor uptake values at 4 h after injection ($P > 0.05$; Table 1). However, ^{111}In-DOTA-Re(Arg^{11})CCMSH exhibited a significantly higher tumor uptake value than that of ^{99m}Tc-(Arg^{11})CCMSH at 24 h after injection ($P < 0.05$; Table 1), with 8.19 ± 1.63 %ID/g of ^{111}In-DOTA-Re(Arg^{11})CCMSH activity remaining in the tumors. In comparison with ^{99m}Tc-(Arg^{11})CCMSH, ^{111}In-DOTA-Re(Arg^{11})CCMSH exhibited faster whole-body clearance of activity, with approximately 90 %ID washed out of the body by 4 h after injection. Normal organ uptakes of ^{99m}Tc-(Arg^{11})CCMSH and ^{111}In-DOTA-Re(Arg^{11})CCMSH were generally low (<0.9 %ID/g) at 4 h after injection except for the kidneys. The kidney uptake value of ^{99m}Tc-(Arg^{11})CCMSH was significantly lower than that of ^{111}In-DOTA-Re(Arg^{11})CCMSH at 4 and 24 h after injection ($P < 0.05$; Table 1). Renal uptake of ^{99m}Tc-(Arg^{11})CCMSH was 75.0% and 10.6% of that of ^{111}In-DOTA-Re(Arg^{11})CCMSH. High
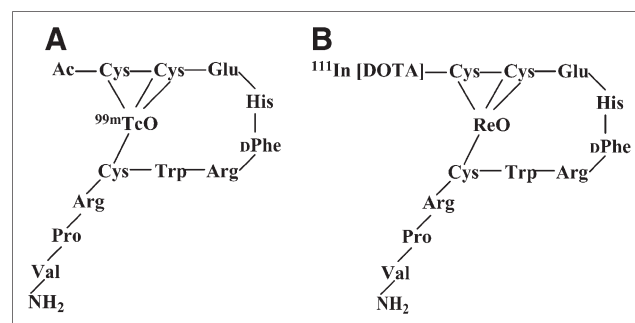
FIGURE 1. Schematic structures of ^{99m}Tc-(Arg^{11})CCMSH (A) and ^{111}In-DOTA-Re(Arg^{11})CCMSH (B).

TABLE 1
Biodistribution Comparison Between 99mTc-(Arg[11])CCMSH and 111In-DOTA-Re(Arg[11])CCMSH in B16/F1 Murine Melanoma-Bearing C57 Mice

	%ID/g						
	99mTc-(Arg[11])CCMSH				111In-DOTA-Re(Arg[11])CCMSH*		
Tissue	1 h	1 h NDP[†]	4 h	24 h	2 h	4 h	24 h
Tumor	14.03 ± 2.58	1.44 ± 0.23	11.16 ± 1.77	3.33 ± 0.50[‡]	17.29 ± 2.49	17.41 ± 5.63	8.19 ± 1.63
Brain	0.04 ± 0.02	0.05 ± 0.03	0.01 ± 0.00	0.00 ± 0.00[‡]	0.03 ± 0.04	0.03 ± 0.07	0.03 ± 0.02
Blood	0.87 ± 0.12	1.14 ± 0.12	0.07 ± 0.01	0.01 ± 0.01[‡]	0.21 ± 0.08	0.09 ± 0.03	0.06 ± 0.04
Heart	0.63 ± 0.17	0.77 ± 0.12	0.07 ± 0.01	0.01 ± 0.01[‡]	0.07 ± 0.09	0.05 ± 0.05	0.36 ± 0.16
Lung	1.52 ± 0.39	2.01 ± 0.13	0.18 ± 0.01[‡]	0.13 ± 0.04	0.30 ± 0.09	0.13 ± 0.04	0.24 ± 0.14
Liver	1.59 ± 0.19	3.38 ± 0.24	0.45 ± 0.12[‡]	0.16 ± 0.14[‡]	0.38 ± 0.04	0.30 ± 0.04	0.32 ± 0.05
Spleen	0.48 ± 0.13	0.84 ± 0.10	0.18 ± 0.03	0.06 ± 0.03[‡]	0.27 ± 0.19	0.27 ± 0.26	0.32 ± 0.25
Stomach	3.00 ± 0.45	0.57 ± 0.14	0.85 ± 0.11[‡]	0.18 ± 0.12	0.23 ± 0.05	0.15 ± 0.10	0.25 ± 0.13
Kidneys	11.66 ± 1.44	12.31 ± 1.66	5.53 ± 1.17[‡]	0.60 ± 0.08[‡]	8.72 ± 1.34	7.37 ± 1.13	5.64 ± 0.52
Muscle	0.23 ± 0.06	0.32 ± 0.10	0.03 ± 0.01	0.01 ± 0.00[‡]	0.03 ± 0.03	0.09 ± 0.07	0.14 ± 0.10
Pancreas	0.33 ± 0.06	0.46 ± 0.06	0.07 ± 0.02[‡]	0.01 ± 0.01[‡]	0.08 ± 0.08	0.02 ± 0.02	0.08 ± 0.05
Bone	0.55 ± 0.11	0.71 ± 0.10	0.09 ± 0.07	0.04 ± 0.01	0.10 ± 0.03	0.19 ± 0.17	0.37 ± 0.02
Skin	1.97 ± 0.37	1.61 ± 0.13	0.18 ± 0.07	0.04 ± 0.01	0.35 ± 0.18	0.20 ± 0.18	0.27 ± 0.06
	%ID						
Intestines	7.32 ± 1.28	4.88 ± 0.49	11.49 ± 2.65	0.32 ± 0.13	0.40 ± 0.04	0.50 ± 0.24	0.56 ± 0.06
Urine	75.77 ± 2.84	77.87 ± 0.94	83.82 ± 3.50	98.17 ± 0.70	91.39 ± 2.11	89.81 ± 4.22	92.65 ± 1.00
	Uptake ratio of tumor/normal tissue						
Tumor/blood	16.13	1.26	159.43	333.00	15.87	193.44	273.00
Tumor/kidneys	1.20	0.12	2.02	5.55	1.98	2.36	1.45
Tumor/liver	8.82	0.43	24.80	20.81	45.50	58.03	25.59
Tumor/muscle	61.00	4.50	372.00	333.00	576.33	193.44	58.50

*Data from (14).
[†]Blocking of tumor uptake by NDP at 1 h after injection.
[‡]$P < 0.05$, significance comparison between 99mTc-(Arg[11])CCMSH and 111In-DOTA-Re(Arg[11])CCMSH at 4 and 24 h after injection.
Data are presented as %ID/g or as %ID (mean ± SD; $n = 4$).

tumor-to-blood and tumor-to-normal organ uptake ratios of 99mTc-(Arg[11])CCMSH and 111In-DOTA-Re(Arg[11])CCMSH were demonstrated at 4 and 24 h after injection (Table 1).

The biodistribution of 99mTc-(Arg[11])CCMSH and 111In-DOTA-Re(Arg[11])CCMSH were determined in B16/F10 pulmonary metastatic murine melanoma-bearing C57 mice and compared with normal C57 mice at 2 and 4 h after injection (Tables 2 and 3). 99mTc-(Arg[11])CCMSH exhibited significantly higher lung uptake values in pulmonary metastatic melanoma-bearing mice than that in normal mice ($P < 0.05$; Table 2) at 2 and 4 h after injection. The 99mTc-(Arg[11])CCMSH radioactivity uptake values of the pulmonary metastatic lung were 5.33 and 3.54 times the lung uptake values of normal lung at 2 and 4 h after injection, respectively. 99mTc-(Arg[11])CCMSH displayed higher lung-to-normal organ uptake ratios in pulmonary metastatic melanoma-bearing mice than those in normal mice (Table 2). 111In-DOTA-Re(Arg[11])CCMSH exhibited significantly higher lung uptake values in pulmonary metastatic melanoma-bearing mice than that in normal mice ($P < 0.05$; Table 3) at 2 and 4 h after injection. The 111In-DOTA-Re(Arg[11])CCMSH radioactivity uptake values of the pulmonary metastatic lung were 39.57 and 96.88 times the

lung uptake values of normal lung at 2 and 4 h after injection, respectively. 111In-DOTA-Re(Arg[11])CCMSH displayed higher lung-to-normal organ uptake ratios in pulmonary metastatic melanoma-bearing mice than those in normal mice (Table 3).

Two B16/F1 flank murine melanoma-bearing C57 mice were injected separately with 99mTc-(Arg[11])CCMSH and 111In-DOTA-Re(Arg[11])CCMSH through the tail vein to visualize the tumors at 2 h after dose administration. The whole-body SPECT images of the mice were fused with the respective CT images. The transaxial tumor images and the whole-body images are presented in Figure 2. The flank melanoma tumors were visualized clearly by both 99mTc-(Arg[11])CCMSH and 111In-DOTA-Re(Arg[11])CCMSH at 2 h after injection. Both 99mTc-(Arg[11])CCMSH and 111In-DOTA-Re(Arg[11])CCMSH exhibited high tumor-to-normal organ uptake ratios except for the kidney, which were coincident with the trend observed in the biodistribution results of 99mTc-(Arg[11])CCMSH and 111In-DOTA-Re(Arg[11])CCMSH.

B16/F10 pulmonary melanoma-bearing C57 mice were injected with 99mTc-(Arg[11])CCMSH and 111In-DOTA-Re(Arg[11])CCMSH through the tail vein to image metastatic

TABLE 2

TABLE 2
Biodistribution of ^{99m}Tc-(Arg^{11})CCMSH in Normal and B16/F10 Lung Metastatic Mice

| | %ID/g | | | |
| | 2 h | | 4 h | |
Tissue	Lung metastases	Normal	Lung metastases	Normal
Lung	2.77 ± 0.98*	0.52 ± 0.22	2.30 ± 1.78*	0.65 ± 0.13
Brain	0.02 ± 0.03	0.08 ± 0.07	0.06 ± 0.07	0.10 ± 0.09
Blood	0.39 ± 0.09	0.36 ± 0.07	0.37 ± 0.21	0.19 ± 0.01
Heart	0.46 ± 0.30	0.44 ± 0.27	0.50 ± 0.48	0.26 ± 0.03
Kidney	9.64 ± 0.64	10.20 ± 1.18	6.77 ± 1.08	5.84 ± 0.62
Liver	1.14 ± 0.15	0.94 ± 0.29	0.63 ± 0.23	0.63 ± 0.10
Muscle	0.24 ± 0.18	0.44 ± 0.27	0.46 ± 0.22	0.34 ± 0.31
Spleen	0.45 ± 0.35	0.26 ± 0.23	0.40 ± 0.43	0.85 ± 0.76
Stomach	1.28 ± 0.42	1.65 ± 0.66	0.95 ± 0.24*	0.23 ± 0.03
Pancreas	0.17 ± 0.16	0.17 ± 0.09	0.33 ± 0.15*	0.00 ± 0.00
		%ID		
Intestine	9.53 ± 1.23	9.77 ± 1.01	11.75 ± 2.60	9.98 ± 2.17
Urine	81.87 ± 1.98	81.58 ± 3.06	82.70 ± 3.18	85.44 ± 1.40
		Uptake ratio of tumor/normal tissue		
Lung/blood	7.10	1.44	6.22	3.42
Lung/kidneys	0.29	0.05	0.34	0.11
Lung/liver	2.43	0.55	3.65	1.03
Lung/muscle	11.54	1.18	5.00	1.91

*$P < 0.05$, significance comparison between ^{99m}Tc-(Arg^{11})CCMSH in pulmonary metastatic melanoma mouse model and ^{99m}Tc-(Arg^{11})CCMSH in normal mouse model.

Data are presented as %ID/g or as %ID (mean ± SD; $n = 4$).

melanoma deposits. The SPECT data acquisition started at 2 h after the dose administration. The whole-body SPECT images of the mice were fused separately with CT images. The transaxial tumor images and the whole-body images are presented in Figure 2. The pulmonary metastatic melanoma lesions were clearly imaged by both ^{99m}Tc-(Arg^{11})CCMSH and ^{111}In-DOTA-Re(Arg^{11})CCMSH. Distinct metastatic focal deposits were visible in transaxial images sections with ^{99m}Tc-(Arg^{11})CCMSH.

DISCUSSION

The development of small-animal imaging techniques makes it possible for researchers to image the biochemical processes in small-animal models of disease noninvasively. MRI and CT allow collection of high-resolution anatomic data but yield limited data on biologic function. SPECT and PET can yield important functional data but lack high spatial resolution. Dual-modality imaging, which combines MRI or CT with SPECT or PET through data coregistration, is a powerful tool for correlating structural and functional imaging information. In this study, dual-modality micro-SPECT/CT was used to detect melanoma tumors in mouse animal models. Radiolabeled (Arg^{11})CCMSH peptide analogs were used to target MC1 receptors present on melanoma tumors. Coregistration of micro-CT data with micro-SPECT

data allowed accurate identification and localization of the melanoma tumors.

Primary flank melanoma tumors were clearly visualized by both ^{99m}Tc-(Arg^{11})CCMSH and ^{111}In-DOTA-Re(Arg^{11})-CCMSH at 2 h after injection on SPECT/CT images (Fig. 2). SPECT of tumors accurately matched the anatomic information from CT images. However, similar tissue densities between tumor tissue and surrounding muscle tissue would make detection of small tumors difficult by micro-CT alone. Moreover, it is likely that detection of metastatic deposits in the body cavity by micro-CT would face similar challenges without the addition of a contrast agent. The radioactivity uptakes in normal organs such as the lung and liver were very low except for the kidneys, which was the primary excretion pathway of the peptides.

The biodistribution of ^{99m}Tc-(Arg^{11})CCMSH and ^{111}In-DOTA-Re(Arg^{11})CCMSH in the B16/F10 pulmonary melanoma model demonstrated that both ^{99m}Tc- and ^{111}In-labeled peptides displayed significantly higher uptakes in metastatic lungs compared with normal lungs ($P < 0.05$). The biodistribution results were coincident with SPECT/CT images in the B16/F10 pulmonary metastatic melanoma model (Fig. 2). Pulmonary metastatic melanoma deposits were initially detectable by micro-CT approximately 15–18 d after tail vein inoculation of B16/F10 melanoma cells (24). The air space in the lungs was in high contrast with tumor-tissue-yield diagnostic images of metastatic

TABLE 3
Biodistribution of ^{111}In-DOTA-Re(Arg^{11})CCMSH in Normal and B16/F10 Lung Metastatic Mice

| | %ID/g | | | |
| | 2 h | | 4 h | |
Tissue	Lung metastases	Normal	Lung metastases	Normal
Lung	9.10 ± 2.86*	0.23 ± 0.05	7.75 ± 3.66*	0.08 ± 0.03
Brain	0.03 ± 0.02	0.02 ± 0.01	0.02 ± 0.02	0.00 ± 0.00
Blood	0.37 ± 0.21*	0.10 ± 0.06	0.10 ± 0.06	0.05 ± 0.05
Heart	0.11 ± 0.06	0.06 ± 0.04	0.09 ± 0.04	0.04 ± 0.05
Kidney	8.37 ± 1.76*	6.16 ± 0.70	6.45 ± 2.33	7.31 ± 0.57
Liver	0.46 ± 0.11	0.38 ± 0.06	0.37 ± 0.10	0.32 ± 0.04
Muscle	0.07 ± 0.04	0.03 ± 0.03	0.04 ± 0.02	0.02 ± 0.03
Spleen	0.24 ± 0.08	0.11 ± 0.12	0.09 ± 0.04*	0.02 ± 0.03
Stomach	0.28 ± 0.11	0.30 ± 0.05	0.14 ± 0.09	0.12 ± 0.05
Pancreas	0.27 ± 0.24	0.05 ± 0.04	0.05 ± 0.02*	0.03 ± 0.01
Bone	0.23 ± 0.06	0.07 ± 0.03	0.07 ± 0.05	0.04 ± 0.09
	%ID			
Intestine	0.42 ± 0.10	0.42 ± 0.07	0.35 ± 0.05	0.36 ± 0.13
Urine	90.93 ± 3.27	96.24 ± 0.38	92.06 ± 3.82	96.08 ± 0.22
	Uptake ratio of tumor/normal tissue			
Lung/blood	24.59	2.30	77.50	1.60
Lung/kidneys	1.09	0.04	1.20	0.01
Lung/liver	19.78	0.61	20.95	0.25
Lung/muscle	130.00	3.29	193.75	4.00

*$P < 0.05$, significance comparison between ^{111}In-DOTA-Re(Arg^{11})CCMSH in pulmonary metastatic melanoma mouse model and ^{111}In-DOTA-Re(Arg^{11})CCMSH in normal mouse model.

Data are presented as %ID/g or as %ID (mean ± SD; $n = 4$).

melanoma. The growth of metastatic melanoma in the lungs could be monitored with additional CT studies over time. Pulmonary metastatic melanoma lesions were clearly imaged using micro-SPECT with both ^{99m}Tc-(Arg^{11})CCMSH and ^{111}In-DOTA-Re(Arg^{11})CCMSH at 2 h after injection. Individual metastatic foci were not resolvable with ^{111}In-DOTA-Re(Arg^{11})CCMSH, whereas several metastatic deposits were identified with ^{99m}Tc-(Arg^{11})CCMSH. The higher imaging resolution of ^{99m}Tc-(Arg^{11})CCMSH is likely due to the superior imaging decay characteristics of ^{99m}Tc. Theoretically, the imaging of metastatic melanoma lesions in the early stage of development seems possible
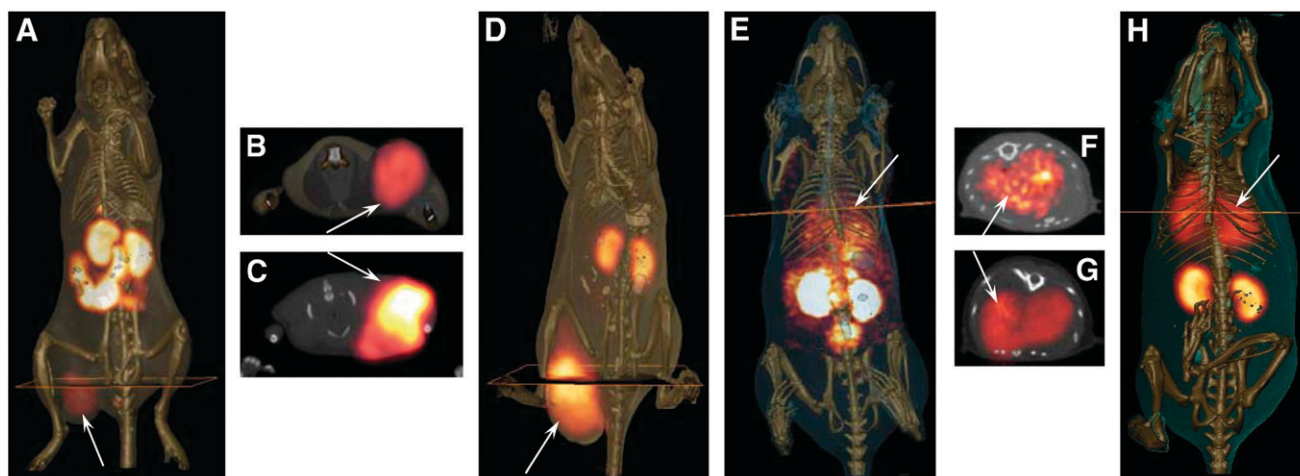
FIGURE 2. Whole-body and transaxial images of ^{99m}Tc-(Arg^{11})CCMSH (A and B, respectively) and ^{111}In-DOTA-Re(Arg^{11})CCMSH (D and C, respectively) in B16/F1 flank melanoma-bearing C57 mice at 2 h after injection. Whole-body and transaxial images of ^{99m}Tc-(Arg^{11})CCMSH (E and F, respectively) and ^{111}In-DOTA-Re(Arg^{11})CCMSH (H and G, respectively) in B16/F10 pulmonary metastatic melanoma-bearing C57 mice 2 h after injection.

because the spatial resolution of SPECT with the pinhole collimator is approximately 1.6 mm for the Jaszczak phantom filled with ^{99m}Tc or ^{111}In aqueous solution. However, on the basis of individual planar images, the smallest metastatic deposits detected with ^{99m}Tc-(Arg^{11})CCMSH were approximately 2.0 mm in diameter (image not shown). The localization and diameter of individual metastases were confirmed on necropsy after completion of the imaging study.

Currently, ^{18}F-FDG is the most commonly used imaging agent for melanoma staging and the identification of metastases in the clinic. Melanoma tumors are in a high metabolic state and tend to import and trap ^{18}F-FDG. However, ^{18}F-FDG is not a melanoma-specific imaging agent and also is not effective in imaging melanomas that have primary energy sources other than glucose (6). Radiolabeled α-MSH peptide analogs are melanoma selective and could be used to noninvasively confirm the identity of a tumor as melanoma or be used in cases in which ^{18}F-FDG uptake is not optimal. Moreover, radiolabeled α-MSH peptide analogs as imaging agents may have their greatest utility when used in a "matched-pair" approach for melanoma radiotherapy. In a matched-pair approach to radiotherapy, the same melanoma-targeting peptide can be radiolabeled with radionuclides possessing diagnostic imaging or therapeutic decay properties. The advantage of this approach is that patient-specific dosimetry can be determined using the imaging agent so that the optimal dose of the peptide radiolabeled with the therapeutic radionuclide can be administered.

Metastatic melanoma is resistant to current chemotherapy and immunotherapy regimens and the survival times for patients with disseminated metastatic melanoma average 3–15 mo (2). There is a critical need for new and efficacious treatments for advanced stage melanoma. Recent preclinical therapy results using ^{188}Re-(Arg^{11})CCMSH and ^{212}Pb-DOTA-Re(Arg^{11})CCMSH highlight the potential of peptide-targeted radiotherapy of melanoma. ^{99m}Tc-(Arg^{11})CCMSH and ^{111}In-DOTA-Re(Arg^{11})CCMSH could be used as matched-pair imaging agents for ^{188}Re-(Arg^{11})CCMSH and ^{212}Pb-DOTA-ReCCMSH(Arg^{11}). Both ^{188}Re-(Arg^{11})CCMSH and ^{212}Pb-DOTA-Re(Arg^{11})CCMSH exhibited therapeutic efficacy in mouse melanoma therapy studies (15,16). ^{212}Pb-DOTA-Re(Arg^{11})CCMSH yielded the highest therapeutic efficacy, with 45% of the melanoma mice exhibiting complete remissions and surviving the therapy study disease free (16). Closely matched imaging agents are necessary for ^{188}Re-(Arg^{11})CCMSH and ^{212}Pb-DOTA-Re(Arg^{11})CCMSH if either one is to make a successful translation into the clinic.

Both ^{99m}Tc-(Arg^{11})CCMSH and ^{111}In-DOTA-Re(Arg^{11})-CCMSH exhibited favorable pharmacokinetics and tumor-targeting properties in B16/F1 murine melanoma-bearing C57 mice (Table 1). Froidevaux et al. (25–27) reported 2 novel DOTA-conjugated MSH analogs based on the high-affinity NDP MSH sequence. ^{111}In-DOTA-NAPamide

displayed higher tumor uptake values and better pharmacokinetics than ^{111}In-DOTA-MSH$_{(oct)}$. The tumor uptake values of ^{111}In-DOTA-NAPamide were 7.56 ± 0.51 %ID/g at 4 h and 2.32 ± 0.28 %ID/g at 24 h after injection in the B16/F1 murine melanoma mouse model (27). In comparison with ^{111}In-DOTA-NAPamide, both ^{99m}Tc-(Arg^{11})CCMSH and ^{111}In-DOTA-Re(Arg^{11})CCMSH exhibited superior receptor-mediated tumor uptake values and tumor-to-kidney uptake ratios in the same tumor-bearing mouse model. ^{99m}Tc-(Arg^{11})CCMSH exhibited 1.48 and 1.44 times the tumor uptake value of ^{111}In-DOTA-NAPamide at 4 and 24 h after injection. Furthermore, ^{99m}Tc-(Arg^{11})CCMSH exhibited 1.35 and 6.34 times the tumor-to-kidney uptake ratio of ^{111}In-DOTA-NAPamide at 4 and 24 h after injection. ^{111}In-DOTA-Re(Arg^{11})CCMSH exhibited 2.30 and 3.52 times the tumor uptake value of ^{111}In-DOTA-NAPamide at 4 and 24 h after injection. Moreover, ^{111}In-DOTA-Re(Arg^{11})CCMSH displayed 1.33 and 2.70 times the tumor-to-kidney uptake ratio of ^{111}In-DOTA-NAPamide at 4 and 24 h after injection. It is likely that structural differences—namely, metal cyclization—are responsible for the superior radioactivity uptake and retention properties of the ^{99m}Tc-(Arg^{11})CCMSH and ^{111}In-DOTA-Re(Arg^{11})-CCMSH peptides in melanoma tumors.

CONCLUSION

^{99m}Tc-(Arg^{11})CCMSH and ^{111}In-DOTA-Re(Arg^{11})CCMSH exhibited high melanoma uptake in both primary and pulmonary metastatic melanoma tumors coupled with favorable pharmacokinetics, highlighting their potential as novel imaging probes for both primary and metastatic melanoma detection. In combination with SPECT/CT equipment, ^{99m}Tc-(Arg^{11})CCMSH and ^{111}In-DOTA-Re(Arg^{11})CCMSH could provide an effective approach to noninvasively monitor the development of the melanoma tumors in vivo.

REFERENCES

1. Jemal A, Siegel R, Ward E, et al. Cancer statistics, 2006. *CA Cancer J Clin.* 2006; 56:106–130.
2. Balch CM, Soong SJ, Gershenwald JE, et al. Prognostic factors analysis of 17,600 melanoma patients: validation of the American Joint Committee on Cancer Melanoma Staging System. *J Clin Oncol.* 2001;19:3622–3634.
3. Wang SQ, Rabinovitz H, Kopf AW, Oliviero M. Current technologies for the in vivo diagnosis of cutaneous melanomas. *Clin Dermatol.* 2004;22:217–222.
4. Nabi HA, Zubeldia JM. Clinical application of ^{18}F-FDG in oncology. *J Nucl Med Technol.* 2002;30:3–9.
5. Som P, Atkins HL, Bandoypadhyay D, et al. A fluorinated glucose analogue, 2-fluoro-2-deoxy-D-glucose (F-18): nontoxic tracer for rapid tumor detection. *J Nucl Med.* 1980;21:670–675.

6. Dimitrakopoulou-Strauss A, Strauss LG, Burger C. Quantitative PET studies in pretreated melanoma patients: a comparison of 6-[^{18}F]fluoro-L-DOPA with ^{18}F-FDG and ^{15}O-water using compartment and non-compartment analysis. *J Nucl Med.* 2001;42:248–256.

7. Tatro JB, Reichlin S. Specific receptors for alpha-melanocyte-stimulating hormone are widely distributed in tissues of rodents. *Endocrinology.* 1987;121:1900–1907.

8. Siegrist W, Solca F, Stutz S, et al. Characterization of receptors for alpha-melanocyte-stimulating hormone on human melanoma cells. *Cancer Res.* 1989;49:6352–6358.

9. Giblin MF, Wang NN, Hoffman TJ, Jurisson SS, Quinn TP. Design and characterization of α-melanotropin peptide analogs cyclized through rhenium and technetium metal coordination. *Proc Natl Acad Sci U S A.* 1998;95:12814–12818.

10. Chen J, Cheng Z, Hoffman TJ, Jurisson SS, Quinn TP. Melanoma-targeting properties of ^{99m}technetium-labeled cyclic α-melanocyte-stimulating hormone peptide analogues. *Cancer Res.* 2000;60:5649–5658.

11. Miao Y, Owen NK, Whitener D, Gallazzi F, Hoffman TJ, Quinn TP. In vivo evaluation of ^{188}Re-labeled alpha-melanocyte stimulating hormone peptide analogs for melanoma therapy. *Int J Cancer.* 2002;101:480–487.

12. Miao Y, Whitener D, Feng W, Owen NK, Chen J, Quinn TP. Evaluation of the human melanoma targeting properties of radiolabeled alpha-melanocyte stimulating hormone peptide analogues. *Bioconjug Chem.* 2003;14:1177–1184.

13. Chen J, Cheng Z, Owen NK, et al. Evaluation of an ^{111}In-DOTA-rhenium cyclized α-MSH analog: a novel cyclic-peptide analog with improved tumor-targeting properties. *J Nucl Med.* 2001;42:1847–1855.

14. Cheng Z, Chen J, Miao Y, Owen NK, Quinn TP, Jurisson SS. Modification of the structure of a metallopeptide: synthesis and biological evaluation of ^{111}In-labeled DOTA-conjugated rhenium-cyclized α-MSH analogues. *J Med Chem.* 2002;45:3048–3056.

15. Miao Y, Owen NK, Fisher DR, Hoffman TJ, Quinn TP. Therapeutic efficacy of a ^{188}Re labeled α-melanocyte stimulating hormone peptide analogue in murine and human melanoma-bearing mouse models. *J Nucl Med.* 2005;46:121–129.

16. Miao Y, Hylarides M, Fisher DR, et al. Melanoma therapy via peptide-targeted α-radiation. *Clin Cancer Res.* 2005;11:5616–5621.

17. Ishizu K, Mukai T, Yonekura Y, et al. Ultra-high resolution SPECT system using four pinhole collimators for small animal studies. *J Nucl Med.* 1995;36:2282–2287.

18. Jaszczak RJ, Li J, Wang H, Zalutsky MR, Coleman RE. Pinhole collimation for ultra-high resolution, small field-of-view SPECT. *Phys Med Biol.* 1994;39:425–437.

19. Strand SE, Ivanovich M, Erlandsson K, et al. Small animal imaging with pinhole single photon emission computed tomography. *Cancer.* 1994;73:981–984.

20. Weber DA, Ivanivich M, Franceschi D, et al. Pinhole SPECT: an approach to in vivo high resolution SPECT imaging in small laboratory animals. *J Nucl Med.* 1994;35:342–348.

21. Weber DA, Ivanovich M. Pinhole SPECT: ultra-high resolution imaging for small animal studies. *J Nucl Med.* 1995;36:2287–2289.

22. Yukihiro M, Inoue T, Iwasaki T, Tomiyoshi K, Erlandsson K, Endo K. Myocardial infarction in rats: high resolution single photon emission tomography imaging with a pinhole collimator. *Eur J Nucl Med.* 1996;23:896–900.

23. Weisenberger AG, Wojcik R, Bradley EL, et al. SPECT-CT system for small animal imaging. *IEEE Trans Nucl Sci.* 2003;50:74–79.

24. Winkelmann CT, Figueroa SD, Rold TL, Volkert WA, Hoffman TJ. Micro-imaging characterization of a B16-F10 melanoma metastasis mouse model. *Mol Imaging.* 2006;5:105–114.

25. Froidevaux S, Calame-Christe M, Sumanovski L, Tanner H, Eberle AN. DOTA α-melanocyte-stimulating hormone analogues for imaging metastatic melanoma lesions. *Ann N Y Acad Sci.* 2003;994:378–383.

26. Froidevaux S, Calame-Christe M, Tanner H, Sumanovski L, Eberle AN. A novel DOTA-α-melanocyte-stimulating hormone analog for metastatic melanoma diagnosis. *J Nucl Med.* 2002;43:1699–1706.

27. Froidevaux S, Calame-Christe M, Schuhmacher J, et al. A gallium-labeled DOTA-alpha-melanocyte-stimulating hormone analog for PET imaging of melanoma metastases. *J Nucl Med.* 2004;45:116–123.